Applied Physics Letters

RESEARCH ARTICLE | MAY 05 2026

Thermal transport in γ-InSe: Bulk single crystals and thin flakes

Farjana Ferdous Tonni ; Maliha Maliat ; Sujit Bati; Md Sabbir Akhanda ; Harsh Chandra; Ethan A. Scott ; Abir Hasan ; Sergiy Krylyuk ; Nikhil Shukla ; Costel Constantin; Patrick E. Hopkins ; Junichiro Shiomi ; Albert V. Davydov ; Mona Zebarjadi

Appl. Phys. Lett. 128, 182202 (2026)
https://doi.org/10.1063/5.0324196

AIP Publishing

Applied Physics Letters ARTICLE pubs.aip.org/aip/apl

Thermal transport in γ-InSe: Bulk single crystals and thin flakes

Cite as: Appl. Phys. Lett. **128**, 182202 (2026); doi: 10.1063/5.0324196
Submitted: 22 January 2026 · Accepted: 6 April 2026 ·
Published Online: 5 May 2026

View Online Export Citation CrossMark

Farjana Ferdous Tonni,[1] Maliha Maliat,[1] Sujit Bati,[2] Md Sabbir Akhanda,[1] Harsh Chandra,[3] Ethan A. Scott,[4] Abir Hasan,[1] Sergiy Krylyuk,[5] Nikhil Shukla,[1] Costel Constantin,[6] Patrick E. Hopkins,[2,4,7] Junichiro Shiomi,[3,8] Albert V. Davydov,[5] and Mona Zebarjadi[1,2,7,a)]

AFFILIATIONS

[1]Department of Electrical and Computer Engineering, University of Virginia, Charlottesville, Virginia 22904, USA
[2]Department of Physics, University of Virginia, Charlottesville, Virginia 22904, USA
[3]Institute of Engineering Innovation, University of Tokyo, Tokyo 113-8656, Japan
[4]Department of Mechanical and Aerospace Engineering, University of Virginia, Charlottesville, Virginia 22904, USA
[5]Material Science and Engineering Division, National Institute of Standards and Technology, Gaithersburg, Maryland 20899, USA
[6]Department of Physics and Astronomy, James Madison University, Harrisonburg, Virginia 22807, USA
[7]Department of Materials Science and Engineering, University of Virginia, Charlottesville, Virginia 22904, USA
[8]Department of Mechanical Engineering, University of Tokyo, Tokyo 113-8656, Japan

[a)]**Author to whom correspondence should be addressed:** mz6g@virginia.edu

ABSTRACT

We measure the temperature-dependent in-plane thermal conductivity, $\kappa_{\parallel}(T)$, of high-purity γ-InSe bulk single crystals and exfoliated thin flakes (30–50 nm) from 50 to 300 K. Our bulk results agree with prior bulk reports and provide a reproducible reference for phonon transport. In the literature, cross-plane thermal conductivity of supported InSe flakes shows relatively modest variation, whereas reported room-temperature in-plane values for supported flakes span a wide range, including outliers that exceed bulk despite much smaller thickness. In our measurements, the flake $\kappa_{\parallel}$ at room temperature is lower than bulk, as expected, but exhibits substantial sample-to-sample variability; despite being thinner, intrinsic flakes show higher $\kappa_{\parallel}$ than doped flakes, consistent with reduced impurity scattering and improved flake uniformity. We analyze our data using a Callaway-type phonon-scattering model in which substrate interactions (including plausible strain-related renormalization of acoustic parameters) contribute to the observed spread near room temperature. However, below ~150 K, the measured trends cannot be captured without invoking changes in sound velocity far larger than realistic strain levels, indicating that additional mechanisms beyond simple strain renormalization are required at low temperature. These measurements provide low-temperature $\kappa_{\parallel}$ benchmarks for γ-InSe flakes and constrain how much of the reported room-temperature spread can be explained by thickness, nonuniformity, and substrate effects alone.

Two-dimensional (2D) layered materials are promising for nanoscale and flexible electronics because of their distinctive mechanical, thermal, and electronic properties. They consist of atomically thin layers held together by weak van der Waals interactions in the out-of-plane direction, while strong covalent bonding connects atoms within each layer. This structural anisotropy, including in III–VI metal monochalcogenides (MX; M = Ga, In; X = S, Se, Te), leads to strongly anisotropic thermal conductivity, κ. Consequently, these materials have been proposed as anisotropic interfacial layers that spread heat laterally while limiting cross-plane heat exchange between a device and its substrate when such coupling is undesirable.[1,2] Among this class, indium selenide (InSe) has attracted considerable attention in electronics, optoelectronics, and spintronics owing to its high electron mobility,[3–6] moderate bandgap,[7,8] high photoresponsivity,[9–11] and strong spin–orbit coupling.[12,13] In addition, InSe is mechanically compliant; transferring onto dissimilar substrates can introduce built-in (residual) biaxial strain.[14] Because strain perturbs phonon velocities and scattering pathways, in-plane thermal conductivity can be modulated, providing a practical handle for heat management in device stacks. Motivated by these considerations, we measure the temperature-dependent thermal conductivity of γ-InSe bulk single crystals and exfoliated thin flakes. In what follows, we first present the bulk single-crystal

measurements and analysis; the resulting room-temperature values are consistent with prior bulk reports. We then report cross-plane thermal conductivity measurements for supported flakes, which show comparatively modest sample-to-sample variation. Finally, we address in-plane heat transport in flakes: while published room-temperature $\kappa_{\parallel}$ values for supported flakes span a wide range, sometimes exceeding bulk values, our measured $\kappa_{\parallel}$ at room temperature remain consistent with the bulk benchmark. By combining bulk and flake measurements under comparable conditions, we systematically assess the roles of thickness, roughness, and substrate effects in determining $\kappa_{\parallel}$. In addition, we extend $\kappa_{\parallel}$(T) measurements to low temperatures, providing constraints on phonon transport mechanisms in γ-InSe.

Thermal transport in rhombohedral indium selenide (γ-InSe) bulk single crystals has been investigated previously. Reported room-temperature in-plane thermal conductivities fall in the range of $\sim$9–12 $\mathrm{W\,m^{-1}\,K^{-1}}$, while the cross-plane component is typically $\sim$1.7 $\mathrm{W\,m^{-1}\,K^{-1}}$.[15–18] The relatively small spread among these bulk values (Fig. 1) likely reflects differences in crystal quality and surface condition, including impurity levels and roughness. We use this literature range as a benchmark and begin by presenting our bulk single-crystal measurements.

InSe single crystals were grown using the vertical Bridgman method (details in the supplementary material). The *n*-type samples were doped with 5 at. % Sn. X-ray diffraction and annular dark-field STEM confirmed the γ-InSe crystal phase.[22–24] Room-temperature carrier concentration and mobility, obtained from Hall measurements, are 4×10^{13} $\mathrm{cm^{-3}}$ with $\mu = 534\,\mathrm{cm^2\,V^{-1}\,s^{-1}}$ for undoped InSe, and 3.5×10^{16} $\mathrm{cm^{-3}}$ with $\mu = 782\,\mathrm{cm^2\,V^{-1}\,s^{-1}}$ for Sn-doped InSe.

Here, we study two bulk single-crystal samples: an intrinsic γ-InSe crystal with a thickness of 0.17 mm and an *n*-doped InSe crystal with an average thickness of 0.82 mm. As shown in Fig. S2 in the supplementary material, the crystal surfaces have pronounced thickness nonuniformity and macroscopic height variations. The thickness variations are estimated to be 0.05 and 0.179 mm, corresponding to relative thickness uncertainties of ≈29.4% for the intrinsic sample and ≈21.9% for the *n*-type sample, respectively. Thermal conductivity of the bulk samples was measured using the thermal transport option of a Quantum Design VERSALAB system.

Figure 2 shows the temperature-dependent thermal conductivity of the intrinsic and *n*-type γ-InSe bulk crystals studied here. The electronic contribution, κ_e, estimated at 300 K from the Wiedemann–Franz law, is $\approx 2.5 \times 10^{-6}$ $\mathrm{W\,m^{-1}\,K^{-1}}$ for intrinsic InSe and $\approx 3.2 \times 10^{-3}$ $\mathrm{W\,m^{-1}\,K^{-1}}$ for Sn-doped InSe. Both values are far smaller than the measured total thermal conductivity, indicating that heat transport in γ-InSe is dominated by phonons. The intrinsic bulk $\kappa_{\parallel}(T)$ is consistent with prior reports and remains larger than the cross-plane component.[16] The reported κ values carry an estimated systematic uncertainty of $\approx 20\% - 30\%$ due to thickness nonuniformity. Within our measurement range, we do not observe a low-temperature peak in $\kappa_{\parallel}(T)$. In contrast, Zhang *et al.* reported a peak near 50 K in flexible bulk InSe samples.[18] Differences in sample quality and geometry (e.g., defect density, surface condition, and finite-size effects) may contribute to the lower overall κ values and the presence of a peak in that work.

The thermal conductivity reported in Fig. 2 follows an approximate $1/T$ trend over much of the measured range, consistent with phonon–phonon (Umklapp) scattering dominating heat transport at elevated temperatures. To interpret the observed $\kappa(T)$ behavior, we fit the experimental data using the Callaway model.[25] Within this framework, the thermal conductivity is expressed as

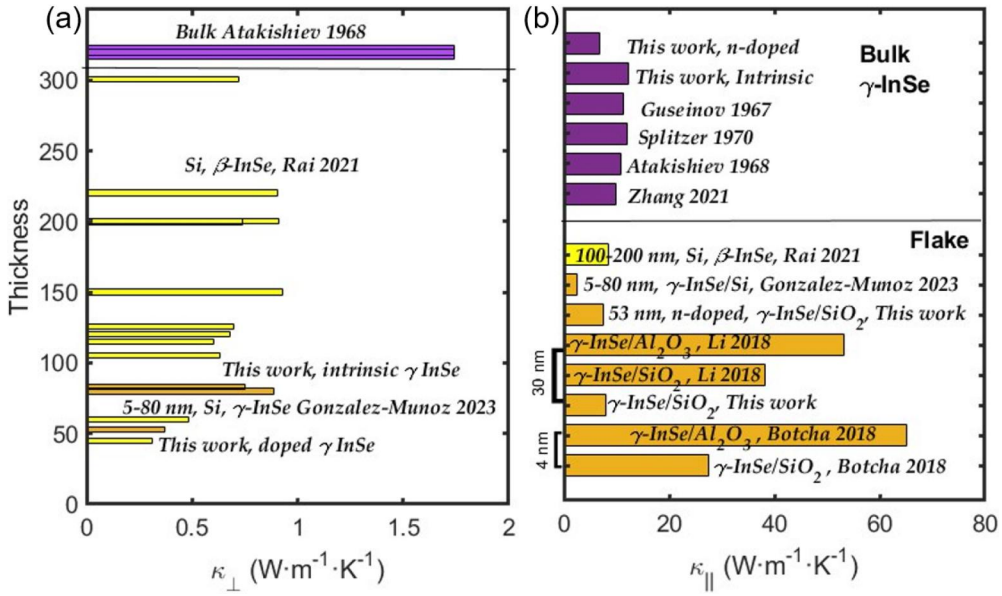

FIG. 1. Comparison of room-temperature cross-plane ($\kappa_{\perp}$) and in-plane thermal conductivity ($\kappa_{||}$) values of γ-InSe and β-InSe from this work and the literature. (a) Thickness-dependent $\kappa_{\perp}$ values of β-InSe[1] (yellow bars) and γ-InSe (orange bars), including intrinsic (80 nm) and n-doped (53 nm) γ-InSe measured in this work. (b) Reported flake data showing a wide spread: β-InSe (100–200 nm) measured by TDTR[1] on Si shows thickness-independent $\kappa_{||}$, while γ-InSe exhibits strong dependence on thickness, substrate, and measurement technique (TDTR, SThM, and Raman).[19–21] Bulk γ-InSe values (purple bars), including intrinsic and n-doped samples from this work, show greater consistency across studies.[15–18]

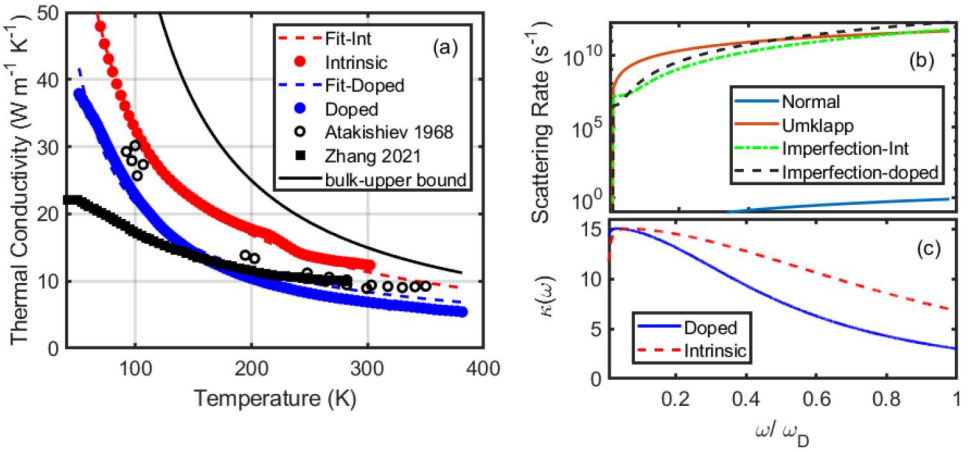

FIG. 2. (a) Temperature-dependent in-plane thermal conductivity of bulk γ-InSe for intrinsic and doped samples compared with literature data.[16,18] (b) Phonon-scattering rates vs frequency up to the Debye frequency. Imperfection scattering rates reported are a sum of τ_B and τ_I defined in Eqs. (3) and (4), including the effect of impurities, finite size, and roughness. (c) The frequency-dependent spectral lattice thermal conductivities as defined by Mao *et al.*[28]

$$\kappa = \frac{k_B}{2\pi^2 v_s}\left(\frac{k_B T}{\hbar}\right)^3 \left[\mathscr{F}[\tau_c] + \frac{(\mathscr{F}[\tau_c/\tau_N])^2}{\mathscr{F}\left[\frac{1}{\tau_N}\left(1-\frac{\tau_c}{\tau_N}\right)\right]}\right], \tag{1}$$

$$\mathscr{F}[g] \equiv \int_0^{\theta_D/T} g(x)\,\frac{x^4 e^x}{(e^x-1)^2}\,dx, \tag{2}$$

where $x = \hbar\omega/k_B T$, k_B is the Boltzmann constant, ω is the phonon angular frequency, $\hbar$ is the reduced Planck constant, T is the absolute temperature, v_s is the (average) sound velocity, θ_D is the Debye temperature, and τ_c is the total phonon relaxation time.

The total scattering rate $1/\tau_c$ is written using Matthiessen's rule as

$$\frac{1}{\tau_c} = \frac{1}{\tau_B} + \frac{1}{\tau_I} + \frac{1}{\tau_U} + \frac{1}{\tau_N}, \tag{3}$$

or equivalently,

$$\frac{1}{\tau_c} = \frac{v_s}{L}\frac{1-p}{1+p} + A\omega^4 + B_U\omega^2 T e^{-\theta_D/3T} + B_N\omega^2 T^3. \tag{4}$$

Here τ_B, τ_I, τ_U, and τ_N are the boundary, impurity, Umklapp, and normal phonon–phonon scattering times, respectively. L is an effective length scale and p is the specularity parameter ($0 \le p \le 1$). The coefficients A, B_U, and B_N parameterize impurity, Umklapp, and normal scattering, respectively.

The Debye temperature is defined as $\theta_D = v_s \frac{\hbar}{k_B}\left(\frac{6\pi^2 N}{V}\right)^{1/3}$, where N/V is the number density. Following Pandey *et al.*,[26] the longitudinal and transverse sound velocities in γ-InSe are $v_l = 3272$ m/s and $v_t = 1853$ m/s, respectively. Using these values, we obtain an average sound velocity $v_s = 2360$ m/s, corresponding to $\theta_D = 223$ K.

Here, B_U and B_N are fitting coefficients for Umklapp and normal scattering, respectively. We assume these parameters are the same for the intrinsic and doped crystals, while A captures impurity scattering and is therefore allowed to differ between the two samples. Finally, since the samples are nonuniform with micrometer-size height variations (see the supplementary material), we have considered the specularity parameter, p,[27] to be close to zero as the system is at the rough boundary limit, where $\tau_b \sim v/L$.

To reproduce the bulk data consistently, we simultaneously fit the intrinsic and doped samples using the same values of B_U and B_N, while allowing different A values. The effective length scale L is taken as the average thickness of each sample (0.17 mm for the intrinsic sample and 0.82 mm for the doped sample). The best-fit parameters (dashed lines in Fig. 2) are listed in Table I.

The scattering rates extracted from the best-fit parameters are plotted in Fig. 2(b). Within the Callaway framework, the bulk data are reproduced with a minimal contribution from normal scattering, i.e., the fitted $1/\tau_N$ remains small compared to the resistive channels over most of the measured range. Umklapp scattering provides the dominant resistive phonon–phonon contribution at elevated temperatures. For reference, the calculated thermal conductivity, including only phonon–phonon scattering (Umklapp and normal terms, with impurity and boundary scattering neglected), is shown as the solid black line; this curve represents an idealized upper bound for crystals without extrinsic imperfection scattering. At room temperature, this bound is $\sim$15 W m^{-1} K^{-1}. In the measured samples, impurity and boundary scattering (here grouped as "imperfection" scattering) reduce $\kappa(T)$ relative to this idealized limit and, together with Umklapp scattering, control the overall temperature dependence. Consistent with Sn doping, the doped crystal exhibits a larger impurity-scattering contribution. At low frequencies, the intrinsic crystal shows a larger boundary-scattering contribution owing to its smaller thickness (smaller effective L).

Next, we investigate thermal transport in exfoliated thin γ-InSe flakes prepared from bulk crystals on SiO_2/Si substrates. Details of exfoliation, substrate preparation, and structural characterization (optical microscopy, SEM–EDX, and AFM) are provided in the supplementary material. AFM analysis shows that thinner flakes generally exhibit lower RMS surface roughness; within the studied samples, doped flakes are smoother than intrinsic ones.

To measure cross-plane heat transport in supported flakes, the samples were coated with an Al transducer layer and characterized by

TABLE I. Fitting parameters used in Callaway's model for bulk thermal conductivity.

Sample	A (s^3)	B_U (s K^{-1})	B_N (s K^{-3})
Intrinsic	8.6×10^{-43}	2.6×10^{-18}	3.6×10^{-35}
n-doped	2.8×10^{-42}		

time-domain thermoreflectance (TDTR). We obtain a cross-plane thermal conductivity of $\kappa_\perp = 0.70\,\mathrm{W\,m^{-1}\,K^{-1}}$ for an 83 nm intrinsic flake and $\kappa_\perp = 0.37\,\mathrm{W\,m^{-1}\,K^{-1}}$ for a 53 nm n-doped flake. The estimated uncertainty is $\sim 0.06\,\mathrm{W\,m^{-1}\,K^{-1}}$, reflecting measurement repeatability and uncertainty in the interfacial thermal conductance at the metal/flake and flake/substrate interfaces. Compared with the bulk cross-plane value ($\kappa_\perp \approx 1.7\,\mathrm{W\,m^{-1}\,K^{-1}}$; Fig. 1), the reduced $\kappa_\perp$ in flakes is consistent with finite-size effects expected when the thickness approaches or falls below a few hundred nanometers. Overall, our flake $\kappa_\perp$ values are in the range of prior reports for InSe flakes (including studies on the β phase), which show comparatively modest variation and a general decrease in $\kappa_\perp$ with decreasing thickness.[1] Consistent with the strong anisotropy of InSe, $\kappa_\perp$ remains much smaller than $\kappa_\parallel$.

In contrast, reported in-plane thermal conductivity values, $\kappa_\parallel$, of exfoliated or few-layer InSe exhibit a wide spread, arising from differences in thickness, residual strain, substrate interactions, flake size, and measurement techniques, as summarized in Fig. 1. Temperature-dependent Raman thermometry reported $\kappa_\parallel = 27.5\,\mathrm{W\,m^{-1}\,K^{-1}}$ at room temperature for a 4 nm InSe flake on SiO_2 protected by a thin SiO_2 passivation layer.[21] In the same work, replacing SiO_2 with high-K Al_2O_3 increased $\kappa_\parallel$ to $65.1\,\mathrm{W\,m^{-1}\,K^{-1}}$, discussed in terms of substrate-induced compressive strain.[21] Related Raman-based measurements showed that adding an Al_2O_3 capping layer to a 29 nm γ-InSe flake on SiO_2 enhanced $\kappa_\parallel$ from 38.2 to $53.1\,\mathrm{W\,m^{-1}\,K^{-1}}$, attributed to interfacial effects such as interface charges and electron–phonon interactions.[19] In contrast, scanning thermal microscopy (SThM) measurements by Buckley *et al.* suggested comparatively weak heat dissipation in thin InSe flakes relative to SiO_2, implying lower effective in-plane thermal transport.[29] They reported that the thermal conductance decreases as the number of layers ($L \leq 5$) and/or flake area ($A < 2\,\mu\mathrm{m}^2$) decreases, and further showed that the effective thermal transport can be enhanced on a high-K h-BN substrate and suppressed on a low-K PMMA substrate.[29] Taken together, these studies indicate that $\kappa_\parallel$ in 2D InSe can be strongly influenced by substrate/interface effects (including strain and interfacial coupling), flake geometry, and the measurement approach. Raman thermometry is indirect and relies on assumptions about optical absorption, heating profiles, and phonon decay pathways, whereas SThM probes local heat flow and is highly sensitive to boundary scattering and interfacial thermal resistances; such differences can lead to method-dependent systematic shifts in the apparent $\kappa_\parallel$.

In this work, using a consistent SiO_2/Si platform, we measure the room-temperature in-plane thermal conductivity of all flakes to be slightly below $10\,\mathrm{W\,m^{-1}\,K^{-1}}$, comparable to bulk values. Devices for in-plane measurements were fabricated by patterning a metal heater on selected flakes with a Ti/Ni stack; representative optical images are shown in Fig. S4 (supplementary material). Thermal transport was measured by heat diffusion imaging (HDI),[30] with methodology, uncertainty analysis, and fabrication details provided in the supplementary material. Figure 3 shows the temperature-dependent in-plane thermal conductivity, $\kappa_\parallel(T)$, for representative intrinsic and n-doped γ-InSe flakes with thicknesses in the range of 30–50 nm. Over 150–230 K, the extracted $\kappa_\parallel$ values for flakes are slightly higher than the bulk reference; however, this difference is within the combined experimental uncertainty of the bulk and flake measurements and should not be over-interpreted as a robust "super-bulk" effect.

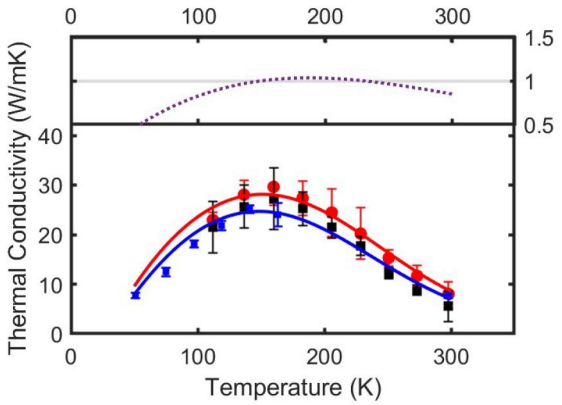

FIG. 3. Temperature-dependent in-plane thermal conductivity of 2D flakes of γ-InSe. Upper part of the plot demonstrates $\alpha(T)$, the scaling factor used to represent the effect of strain. Red circles denote experimental data for an intrinsic flake (30 nm); blue and black squares for two doped flakes, 53 and 37 nm, respectively. Solid red and blue lines are fits for the intrinsic and doped (53 nm) samples, respectively.

We also do not observe a systematic increase in $\kappa_\parallel$ with increasing flake thickness within this limited thickness window. A thickness-independence in the in-plane direction has been reported previously for thicker flakes (100–300 nm);[1] our flakes are thinner than 100 nm, where additional sample-to-sample variability can arise from thickness nonuniformity and substrate interactions (Fig. 1).

To probe potential extrinsic origins of the observed spread, we examined flake morphology by AFM (Fig. S3 in the supplementary material). The supported flakes are comparatively uniform, with nanometer-scale RMS surface roughness ($\eta_{\mathrm{rms}} \lesssim 1$ nm for flakes thinner than 100 nm), and thinner flakes tend to exhibit smaller η_{rms}. In addition, the n-doped flakes consistently show lower $\kappa_\parallel$ than intrinsic flakes of comparable thickness, consistent with enhanced impurity scattering. In the Callaway analysis of the flakes (below), we incorporate surface roughness through a frequency-dependent specularity parameter $p(\omega) = \exp(-4\eta_{\mathrm{rms}}^2\omega^2/v_s^2)$, which provides a convenient way to parameterize the effect of diffuse boundary scattering on $\kappa_\parallel$.

In modeling the flake data, we treat the surface-roughness input as an effective parameter because direct AFM roughness measurements are not available for the specific flakes measured by HDI. We nevertheless constrain this parameter to remain consistent with the nanometer-scale RMS values observed in representative AFM topography (Fig. S3 in the supplementary material). Within these bounds, variations in boundary scattering alone are insufficient to reproduce the full temperature dependence of $\kappa_\parallel(T)$.

A more plausible additional contribution is substrate-induced strain and related substrate interactions in supported flakes. Strain can modify elastic constants and thereby renormalize acoustic phonon velocities, which enter the Callaway model through v_s and θ_D. While we do not directly measure the strain state of each flake, prior Raman studies of γ-InSe on SiO_2/Si report temperature-dependent shifts of phonon peaks, consistent with an evolving strain state with temperature.[14,21] In our analysis, holding v_s and θ_D fixed at the bulk values does not reproduce the flake $\kappa_\parallel(T)$ data. Allowing a temperature-dependent renormalization of v_s (and consequently θ_D)

provides a phenomenological way to capture the observed trends within the Callaway framework [Eqs. (1)–(4)].

We introduce a phenomenological temperature-dependent renormalization of the acoustic velocity through a factor $\alpha(T)$, $v_s(T) = v_{s,\mathrm{bulk}}\ \alpha(T)$, where $\alpha(T) \approx 1$ would correspond to bulk-like acoustic properties. This renormalization may reflect substrate-induced strain and/or interfacial coupling effects in supported flakes. Because multiple quantities in Eqs. (1)–(4) depend on v_s, they are updated consistently when $\alpha(T)$ is introduced. In particular, the Debye temperature scales as $\theta_D \propto v_s$. Within the Debye–Callaway parameterization used here, the impurity and phonon–phonon coefficients scale approximately as $A \propto v_s^{-3}$, $B_N \propto v_s^{-5}$, and $B_U \propto v_s^{-2}$. Strain and substrate coupling may also renormalize anharmonicity; as a first-order approximation, we allow the Grüneisen parameter, γ, to vary inversely with sound velocity, $\gamma \propto 1/v_s$, which enters the Umklapp coefficient through $B_U \propto \gamma^2$.

Figure 3 compares the measured $\kappa_\parallel(T)$ of the InSe flakes with fits obtained from the Callaway analysis. We anchor the scattering parameters to the bulk values and introduce only two additional degrees of freedom for the flakes: (i) a temperature-dependent velocity renormalization factor $\alpha(T)$ and (ii) an effective surface-roughness parameter that controls boundary scattering. The fitted $\alpha(T)$ (upper panel) remains close to unity for $T \gtrsim 100$ K, but decreases to unphysically small values at lower temperatures. Thus, within the present Debye–Callaway framework—even allowing for plausible strain-/substrate-induced renormalization of acoustic parameters—we can capture the high- and intermediate-temperature behavior, but a simple strain-based renormalization is insufficient to reproduce the low-T trends. The in-plane thermal-expansion coefficient of γ-InSe is small (on the order of $10^{-6}\ \mathrm{K}^{-1}$) over the measured temperature range,[31,32] while that of SiO_2 is also small and positive ($\sim 0.5 \times 10^{-6}\ \mathrm{K}^{-1}$).[33] The resulting thermal mismatch yields at most $\sim 0.03\,\% - 0.1\%$ strain upon cooling. Near the Ti/Ni contacts, larger local strain ($\sim$0.2%–0.3%) may occur, but is expected to be partially relaxed and spatially nonuniform. Using the reported Grüneisen parameters ($\gamma \approx 0.65 - 1.38$),[14] this corresponds to a velocity renormalization of $\lesssim 0.5\%$, far smaller than the $\sim$5% reduction implied by $\alpha(T)$ at low temperature. Strain alone, therefore, cannot explain the observed behavior. Resolving this discrepancy will require direct characterization of the strain state in the measured flakes and a more complete assessment (experimental and/or first-principles) of how substrate coupling and strain modify phonon velocities and scattering channels. Consistent with this interpretation, the failure of the Debye–Callaway fit below $\sim$150 K indicates that the low-temperature behavior cannot be described by a spatially uniform renormalization of acoustic velocity alone. A more plausible explanation is additional suppression of long-wavelength heat-carrying phonons in supported flakes, for example, through substrate/interface coupling and defect-related scattering associated with nonuniformity or local disorder. An analogous substrate-induced reduction of in-plane thermal conductivity has been discussed previously for encased graphene[34] and ultrathin graphite, although the detailed phonon physics in γ-InSe is expected to differ. Quantitative separation of these effects in γ-InSe will require thickness-dependent low-temperature measurements and/or microscopic calculations that explicitly include substrate coupling.

Our measurements of intrinsic and n-doped bulk γ-InSe provide a reproducible reference for phonon transport. The temperature dependence of $\kappa(T)$ is captured within a Debye–Callaway analysis using bulk-consistent parameters, with Umklapp and impurity scattering providing the dominant resistive channels over the measured range. Normal scattering contributes only weakly within the present fits, and the intrinsic and doped bulk datasets are reproduced by using shared phonon–phonon parameters (B_U and B_N) while allowing the impurity coefficient A to differ between samples. Optical profilometry further indicates pronounced macroscopic thickness nonuniformity, consistent with predominantly diffuse boundary scattering in the bulk samples.

Against this bulk benchmark, exfoliated flakes on SiO_2/Si exhibit two robust trends. Importantly, these measurements provide systematic, temperature-dependent in-plane $\kappa_\parallel(T)$ for γ-InSe flakes. In contrast to the wide variability reported in the literature, the measured $\kappa_\parallel$ values remain close to the bulk benchmark at room temperature, with deviations that can be partially explained by sample nonuniformity and substrate effects. First, intrinsic flakes show higher $\kappa_\parallel(T)$ than doped flakes despite being thinner, consistent with reduced impurity scattering. Second, within the limited 30–50 nm thickness window studied here, $\kappa_\parallel(T)$ does not increase systematically with thickness, indicating that sample-to-sample variations in uniformity and substrate interactions can compete with simple size effects. Using the bulk parameters as anchors, we obtain good agreement with the flake data at intermediate and high temperatures by introducing a temperature-dependent renormalization factor $\alpha(T)$ for the acoustic velocity (and dependent quantities), together with an effective boundary-scattering parameter. The fitted $\alpha(T)$ remains close to unity above $\sim$100 K but decreases to unphysically small values at lower temperatures, indicating that a simple phenomenological rescaling is insufficient to describe the low-T behavior.

At low temperatures, however, the observed behavior cannot be fully captured within the standard Debye–Callaway framework, indicating the need for additional mechanisms, potentially including temperature-dependent strain and interfacial coupling (e.g., thermal-expansion mismatch, conformity changes), as well as other low-T scattering mechanisms not captured by the model. Future work combining direct strain metrology on the measured devices (e.g., Raman mapping), standardized areal roughness/uniformity characterization, and first-principles calculations of strain-dependent phonon dispersions and anharmonicity should clarify the origin of the low-T trends and reduce reliance on $\alpha(T)$. Overall, our measurements establish low-temperature benchmarks for $\kappa_\parallel(T)$ in γ-InSe flakes and constrain how much of the reported room-temperature spread can be explained by thickness, doping, and substrate/interface quality.

See the supplementary material for the complete details on crystal growth, sample preparation, and device fabrication, as well as measurement methods.

This work was supported in part by NSF (Grant No. 2505197) and the Office of Naval Research (Grant No. N00014-26-1-2076).

Certain commercial equipment, instruments, software, or materials are identified in this paper to specify the experimental procedure adequately. Such identifications are not intended to imply recommendation or endorsement by NIST, nor are they intended to imply that the materials or equipment identified are necessarily the best available for the purpose.

AUTHOR DECLARATIONS

Conflict of Interest

The authors have no conflicts to disclose.

Author Contributions

Farjana Ferdous Tonni: Data curation (equal); Formal analysis (equal); Investigation (equal); Project administration (equal); Resources (equal); Writing – original draft (equal); Writing – review & editing (equal). **Maliha Maliat:** Formal analysis (supporting); Investigation (supporting); Writing – review & editing (supporting). **Sujit Bati:** Investigation (supporting); Resources (supporting). **Md Sabbir Akhanda:** Formal analysis (supporting); Investigation (supporting). **Harsh Chandra:** Formal analysis (supporting); Investigation (supporting). **Ethan A. Scott:** Formal analysis (supporting); Investigation (supporting). **Abir Hasan:** Investigation (supporting); Resources (supporting). **Sergiy Krylyuk:** Investigation (supporting); Resources (supporting); Writing – review & editing (supporting). **Nikhil Shukla:** Supervision (supporting). **Costel Constantin:** Resources (supporting); Supervision (supporting). **Patrick E. Hopkins:** Methodology (supporting); Resources (supporting); Supervision (supporting). **Junichiro Shiomi:** Resources (supporting); Supervision (supporting). **Albert V. Davydov:** Investigation (supporting); Resources (supporting); Writing – review & editing (supporting). **Mona Zebarjadi:** Conceptualization (equal); Formal analysis (equal); Funding acquisition (equal); Supervision (equal); Validation (equal); Visualization (equal); Writing – original draft (equal); Writing – review & editing (equal).

DATA AVAILABILITY

The data that support the findings of this study are openly available in University of Virginia Dataverse at https://doi.org/10.18130/V3/TJTASK, Ref. 35.

REFERENCES

[1]A. Rai, V. K. Sangwan, J. T. Gish, M. C. Hersam, and D. G. Cahill, "Anisotropic thermal conductivity of layered indium selenide," Appl. Phys. Lett. **118**, 073101 (2021).

[2]Y. Cai, M. Faizan, H. Mu, Y. Zhang, H. Zou, H. J. Zhao, Y. Fu, and L. Zhang, "Anisotropic phonon thermal transport in two-dimensional layered materials," Front. Phys. **18**, 43303 (2023).

[3]W. Feng, W. Zheng, W. Cao, and P. Hu, "Back gated multilayer InSe transistors with enhanced carrier mobilities via the suppression of carrier scattering from a dielectric interface," Adv. Mater. **26**, 6587–6593 (2014).

[4]S. Sucharitakul, N. J. Goble, U. R. Kumar, R. Sankar, Z. A. Bogorad, F.-C. Chou, Y.-T. Chen, and X. P. A. Gao, "Intrinsic electron mobility exceeding 10^3 $cm^2/(V\,s)$ in multilayer InSe FETs," Nano Lett. **15**, 3815–3819 (2015).

[5]D. A. Bandurin, A. V. Tyurnina, G. L. Yu, A. Mishchenko, V. Zólyomi, S. V. Morozov, R. K. Kumar, R. V. Gorbachev, Z. R. Kudrynskyi, S. Pezzini, Z. D. Kovalyuk, U. Zeitler, K. S. Novoselov, A. Patanè, L. Eaves, I. V. Grigorieva, V. I. Fal'ko, A. K. Geim, and Y. Cao, "High electron mobility, quantum hall effect and anomalous optical response in atomically thin InSe," Nat. Nanotechnol. **12**, 223–227 (2017).

[6]M. Li, C.-Y. Lin, S.-H. Yang, Y.-M. Chang, J.-K. Chang, F.-S. Yang, C. Zhong, W.-B. Jian, C.-H. Lien, C.-H. Ho, H.-J. Liu, R. Huang, W. Li, Y.-F. Lin, and J. Chu, "High mobilities in layered InSe transistors with indium-encapsulation-induced surface charge doping," Adv. Mater. **30**, 1803690 (2018).

[7]G. W. Mudd, S. A. Svatek, T. Ren, A. Patanè, O. Makarovsky, L. Eaves, P. H. Beton, Z. D. Kovalyuk, G. V. Lashkarev, Z. R. Kudrynskyi, and A. I. Dmitriev, "Tuning the bandgap of exfoliated InSe nanosheets by quantum confinement," Adv. Mater. **25**, 5714–5718 (2013).

[8]Y. Sun, S. Luo, X.-G. Zhao, K. Biswas, S.-L. Li, and L. Zhang, "InSe: A two-dimensional material with strong interlayer coupling," Nanoscale **10**, 7991–7998 (2018).

[9]S. R. Tamalampudi, Y.-Y. Lu, R. K. U, R. Sankar, C.-D. Liao, K. M. B, C.-H. Cheng, F. C. Chou, and Y.-T. Chen, "High performance and bendable few-layered InSe photodetectors with broad spectral response," Nano Lett. **14**, 2800–2806 (2014).

[10]J. Kang, S. A. Wells, V. K. Sangwan, D. Lam, X. Liu, J. Luxa, Z. Sofer, and M. C. Hersam, "Solution-based processing of optoelectronically active indium selenide," Adv. Mater. **30**, 1802990 (2018).

[11]C. Song, S. Huang, C. Wang, J. Luo, and H. Yan, "The optical properties of few-layer InSe," J. Appl. Phys. **128**, 060901 (2020).

[12]K. Premasiri, S. K. Radha, S. Sucharitakul, U. R. Kumar, R. Sankar, F.-C. Chou, Y.-T. Chen, and X. P. A. Gao, "Tuning Rashba spin–orbit coupling in gated multilayer InSe," Nano Lett. **18**, 4403–4408 (2018).

[13]M. Alidoosti, D. N. Esfahani, and R. Asgari, "Charge density wave and superconducting phase in monolayer InSe," Phys. Rev. B **103**, 035411 (2021).

[14]Q. Zhao, T. Wang, R. Frisenda, and A. Castellanos-Gomez, "Giant piezoresistive effect and strong bandgap tunability in ultrathin InSe upon biaxial strain," Adv. Sci. **7**, 2001645 (2020).

[15]G. D. Guseinov, A. I. Rasulov, E. M. Kerimova, and M. Z. Ismailov, "On heat conductivity of $A^{III}B^{VI}$-type semiconductors," Phys. Status Solidi (b) **19**, K7–K10 (1967).

[16]S. M. Atakishiev, D. S. Abdinov, and G. A. Akhundov, "Heat conductivity of indium selenide," Phys. Status Solidi (b) **28**, K47–K50 (1968).

[17]D. Spitzer, "Lattice thermal conductivity of semiconductors: A chemical bond approach," J. Phys. Chem. Solids **31**, 19–40 (1970).

[18]B. Zhang, H. Wu, K. Peng, X. Shen, X. Gong, S. Zheng, X. Lu, G. Wang, and X. Zhou, "Super deformability and thermoelectricity of bulk γ-InSe single crystals," Chin. Phys. B **30**, 078101 (2021).

[19]K. Li, Y.-H. Hong, Z.-W. Li, and X.-K. Liu, "Thermal property engineering of InSe layer by a thin Al_2O_3 stress liner," Appl. Phys. Lett. **113**, 021903 (2018).

[20]S. Gonzalez-Munoz, K. Agarwal, E. G. Castanon, Z. R. Kudrynskyi, Z. D. Kovalyuk, J. Spièce, O. Kazakova, A. Patanè, and O. V. Kolosov, "Direct measurements of anisotropic thermal transport in γ-InSe nanolayers via cross-sectional scanning thermal microscopy," Adv. Mater. Interfaces **10**, 2300081 (2023).

[21]V. D. Botcha, M. Zhang, K. Li, H. Gu, Z. Huang, J. Cai, Y. Lu, W. Yu, and X. Liu, "High-K substrate effect on thermal properties of 2D InSe few layer," J. Alloys Compd. **735**, 594–599 (2018).

[22]J. Miao, C. Leblanc, J. Wang, Y. Gu, X. Liu, B. Song, H. Zhang, S. Krylyuk, W. Hu, A. V. Davydov, T. Back, N. Glavin, and D. Jariwala, "Heterojunction tunnel triodes based on two-dimensional metal selenide and three-dimensional silicon," Nat. Electron. **5**, 744 (2022).

[23]C. Patil, C. Dong, H. Wang, B. M. Nouri, S. Krylyuk, H. Zhang, A. V. Davydov, H. Dalir, and V. J. Sorger, "Self-driven highly responsive p-n junction InSe heterostructure near-infrared light detector," Photonics Res. **10**, A97 (2022).

[24]N. A. Pike, R. Pachter, M. A. Altvater, C. E. Stevens, M. Klein, J. R. Hendrickson, H. Zhang, S. Krylyuk, A. V. Davydov, and N. R. Glavin, "Understanding the origin and implication of the indirect-to-direct bandgap transition in multilayer InSe," J. Phys. Chem. C **128**, 7957 (2024).

[25]J. Callaway, "Model for lattice thermal conductivity at low temperatures," Phys. Rev. **113**, 1046–1051 (1959).

[26]T. Pandey, D. S. Parker, and L. Lindsay, "*Ab initio* phonon thermal transport in monolayer InSe, GaSe, GaS, and alloys," Nanotechnology **28**, 455706 (2017).

[27]J. M. Ziman, *Electrons and Phonons: The Theory of Transport Phenomena in Solids* (Oxford University Press, Oxford, 1960).

[28]D. Mao, J. Yang, M. Han, X. Huang, J. Wang, B. Jia, Z. Wang, X. Xu, L. Xie, Y. Zhou, G. Li, G. W. Ho, and J. He, "Homo-layer flexible Bi_2Te_3-based films with high thermoelectric performance," Sci. Adv. **11**, eadz1019 (2025).

[29]D. Buckley, Z. R. Kudrynskyi, N. Balakrishnan, T. Vincent, D. Mazumder, E. Castanon, Z. D. Kovalyuk, O. Kolosov, O. Kazakova, A. Tzalenchuk, and A. Patanè, "Anomalous low thermal conductivity of atomically thin InSe probed by scanning thermal microscopy," Adv. Funct. Mater. **31**, 2008967 (2021).

[30]T. Zhu, D. H. Olson, P. E. Hopkins, and M. Zebarjadi, "Heat diffusion imaging: In-plane thermal conductivity measurement of thin films in a broad temperature range," Rev. Sci. Instrum. **91**, 113701 (2020).
[31]G. L. Belen'kii, E. Y. Salaev, and R. A. Suleimanov, "Deformation effects in layer crystals," Sov. Phys. Usp. **31**, 434–455 (1988).
[32]I. B. Krynetskii, V. A. Kulbachinskii, N. P. Shabanova, A. V. Tsikunov, R. I. Kovalenko, V. V. Rodin, and S. Y. Gavrilkin, "Anomalous thermal expansion of InSe layered semiconductors in the low-temperature region," J. Exp. Theor. Phys. **116**, 872–875 (2013).
[33]Y. S. Touloukian, R. W. Powel, C. Y. Ho, and P. G. Klemens, "Thermal conductivity of nonmetallic solids," Thermophys. Prop. Matter **2**, 1389 (1970).
[34]W. Jang, Z. Chen, W. Bao, C. N. Lau, and C. Dames, "Thickness-dependent thermal conductivity of encased graphene and ultrathin graphite," Nano Lett. **10**, 3909–3913 (2010).
[35]F. F. Tonni (2026), "Replication data for: Thermal transport in γ-InSe: Bulk single crystals and thin flakes," University of Virginia Dataverse, V. 1, Dataset https://doi.org/10.18130/V3/TJTASK